BNL-222830-2022-COPA

Capacitively Coupled LAPPDs with 2D Pixelated Readout Planes for Time of Flight and Ring Imaging Cherenkov Applications

A. Kiselev

Submitted to the 2021 Nuclear Science Symposium (NSS) and Medical Imaging Conference (MIC), Conference to be held at Yokohama, Tokyo, Japan
October 16 - 23, 2021

Physics Department

Brookhaven National Laboratory

U.S. Department of Energy

USDOE Office of Science (SC), Nuclear Physics (NP) (SC-26)

DISCLAIMER

Capacitively Coupled LAPPDs with 2D Pixelated Readout Planes for Time of Flight and Ring Imaging Cherenkov Applications

A. Kiselev, M. Alfred, R. Alrashidi, A. Alsayegh, M. Aviles, B. Azmoun, S. Butler, M. Chiu, T. Cremer, K. Dehmelt, A. Deshpande, M. Foley, P. Garg, C. Hamel, M. Harvey, X. He, A. Holt, T. K. Hemmick, S. Kuudaar, A. Lyashenko, L. Mwibanda, M. Minot, S. Nelson, S. Park, M. Popecki, M. L. Purschke, C. M. Sarsour, C. Scarlett, B. Schmookler, M. Stochaj, C. Walne, P. Whitney, C. Woody, J. Xie

***Abstract*—Large Area Picosecond Photon Detectors (LAPPDs) are micro-channel plate based photosensors featuring hundreds of square centimeters of sensitive area in a single package and capable of providing timing resolution on the order of 50 ps for single photon detection. However, LAPPDs currently do not exist in finely pixelated 2D readout configurations which, in addition to high-resolution timing, would also provide high spatial resolution required for Ring Imaging CHerenkov (RICH) detectors. One of the recent LAPPD models (Gen II) provides the opportunity to overcome the lack of pixellation by coupling an external readout to the sealed detector itself. The readout plane in this case is a simple printed circuit board (PCB) that can be laid out in a custom application-specific way for 1D or 2D sensitive area pixellation. This allows for a much shorter readout-plane prototyping cycle and provides unprecedented flexibility in choosing an appropriate segmentation that can be optimized for any particular detector need in terms of pad size, orientation, and shape. We fully exploit this feature by designing and testing a variety of readout PCBs with conventional square pads and interleaved anode designs. Data acquired in the lab using a laser system to probe the response of several interleaved and standard pixelated patterns are presented as well as results from a beam test.**

I. Introduction

Large Area Picosecond Photon Detectors (LAPPDs), originally designed by the LAPPD collaboration [1] and now manufactured by Incom Inc. [2], are low profile (~2 cm thick), vacuum sealed, micro-channel plate photomultiplier-based detectors with an active area of up to 20 cm × 20 cm. They offer excellent timing resolution [3], are produced with a variety of transmissive photocathodes with high quantum efficiency (>25 % at 365 nm) and feature high gain (up to ~10^7) and low dark current noise. These devices are nicely suited for high performance ToF and RICH applications. We propose to read out capacitively coupled LAPPDs [4,5] with various square pad and interleaved anode patterns, which enhance charge sharing over more traditional pixelated readouts and deliver spatial resolutions significantly better than the pitch / √ 12. We investigate a broad range of 2D interleaved geometries with varying structural parameters to identify optimal anode designs for specific PID applications. Since the geometric parameters of the anode govern the degree of charge sharing, this procedure allows for the possibility to precisely tune the detector performance, in order to generate a highly isotropic response, with excellent spatial resolution. Furthermore, we focus on the optimization of coarse anode segmentations (with a pixel size up to 5-6 mm), to minimize the channel count and the high costs associated with front end electronics, yet provide sub-mm spatial resolution preferred by a variety of RICH applications.

II. Experimental Setup

Our initial goal was to measure the position resolution capabilities of an LAPPD tile capacitively coupled to an external readout board using a laser beam spot as a reference point. The apparatus is shown in Figure 1, which depicts the LAPPD tile mounted to a readout PCB with both pixelated and interleaved anodes. Charge from the secondary micro-channel gain stage is collected onto a resistive film electrode on the interior bottom of the tile, which then induces a signal on the anode pads of the external PCB. Incom LAPPD tile #97 with a 2mm thick ceramic anode base plate was used. The detector was operated at a potential of 925 V across each micro-channel plate and a potential of 75 V, 200 V, and 250 V was applied respectively in each of the three gaps between the photocathode, two micro-channel plates, and the bottom resistive charge collecting layer.

Manuscript submitted on May 6, 2021. This work was supported in part by the U.S. Department of Energy under Prime Contract No. DE-SC0012704.

J. Xie is with Argonne National Lab, Physics Department

B. Azmoun, M. Chiu, A. Kiselev, M. Purschke, and C. Woody are with Brookhaven National Laboratory, Physics Department, Upton, NY, USA.

M. Sarsour and X. He are with Georgia State University, Physics Department

K. Dehmelt, A. Deshpande, P. Garg, B. Schmookler and T.K. Hemmick are with Stony Brook University, Department of Physics and Astronomy, Stony Brook, NY, USA.

M. Aviles, S. Butler, T. Cremer, M. Foley, C. Hamel, A. Lyashenko, M. Minot, M. Popecki, M. Stochaj, C. Walne, P. Whitney are with Incom Inc., Charlton, MA, USA.

A. Holt is with Howard University, Washington DC, USA.

R. Alrashidi, A. Alsayegh, S. Kuudaar, S. Nelson, L. Mwibanda, C. Scarlett are with Florida A&M University, Tallahassee, FL, USA.

M. Harvey is with Texas Southern University, Houston, TX, USA.

S. Park is with Mississippi State University, Mississippi State, MS, USA.

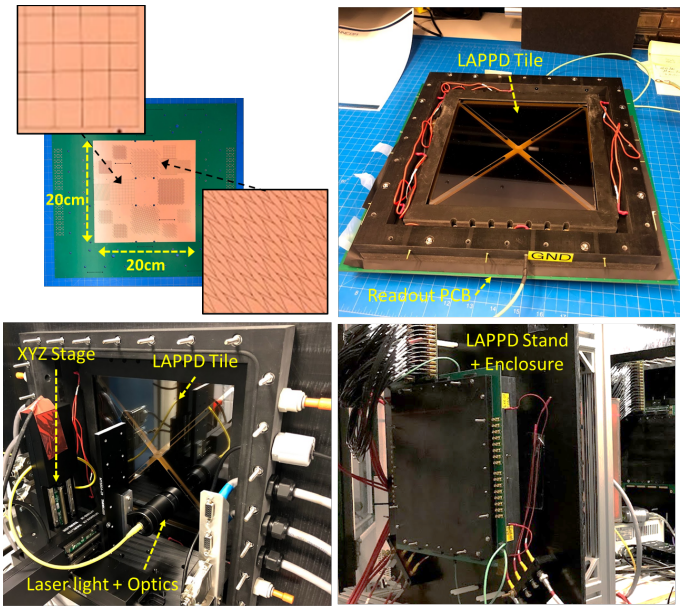

Figure 1 The LAPPD readout PCB consisting of multiple pixelated and interleaved anode patterns is shown in the upper left, and an LAPPD tile mechanically coupled to the readout PCB with a 50 µm thick optically opaque foil sandwiched between them is shown in the upper right. The bottom photos show the LAPPD experimental setup including the LAPPD+PCB module, a laser coupled to a fiber optical cable, the focusing optics, and the LAPPD stand and enclosure.

The setup also includes a 420 nm picosecond laser coupled into a fiber optical cable. Upon exiting the fiber, the laser light is focused by an aspheric 20 mm focal length lens to produce a few dozens of microns diameter RMS beam spot on the LAPPD photocathode, as shown in Figure 2. The residuals from the reconstructed position of the beam spot will ultimately measure the position resolution of the detector. The optical system is mounted to a motorized XYZ-stage in order to position the beam spot over the various anode patterns on the PCB with an

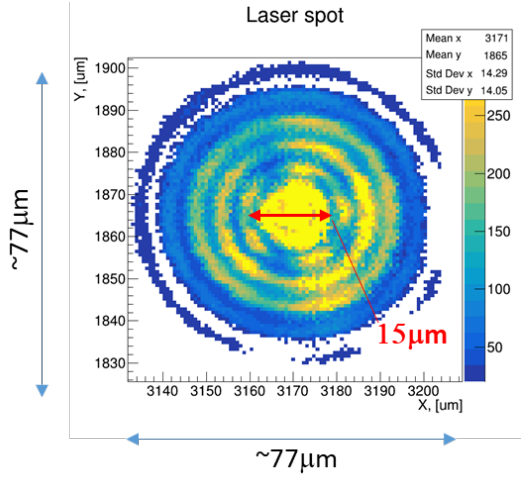

Figure 2 Imaged beam spot from the fiber optical cable after focusing by an aspheric lens, used as a reference for position resolution measurements.

accuracy of about 1µm. Finally, a DAQ system comprises 256 channels of DRS4-based front end electronics (CAEN V1742 digitizers) with a sampling rate of 5 GS/s, connected to the readout boards via six feet long coaxial MCX cables.

III. Lab Results with Laser

Some typical benchtop measurements with a laser photon source are presented here. In the measurements that follow, the beam intensity was lowered by a large factor by an appropriate neutral density filter, such that for the majority of events, single photons arrive at the photocathode for each event trigger.

A. Induced signal spread

The induced signal spread on the readout pads of the external capacitively coupled PCB is illustrated in Figure 3, which shows the results from an 8 × 8 square pixel array. Positioning the laser beam spot between four 6 mm × 6 mm square pads induces 5-10 mV signals on them, which are used to define a single photon cluster by attaching neighbor pixels above threshold to the one with a highest amplitude. The position centroid along both the x- and y-directions is in turn determined from the pad location and corresponding charge amplitudes. Pixel amplitudes are evaluated as a sum over 1 ns window around the peak value. In this case, the cluster is typically contained in a 3 x 3 pixel area.

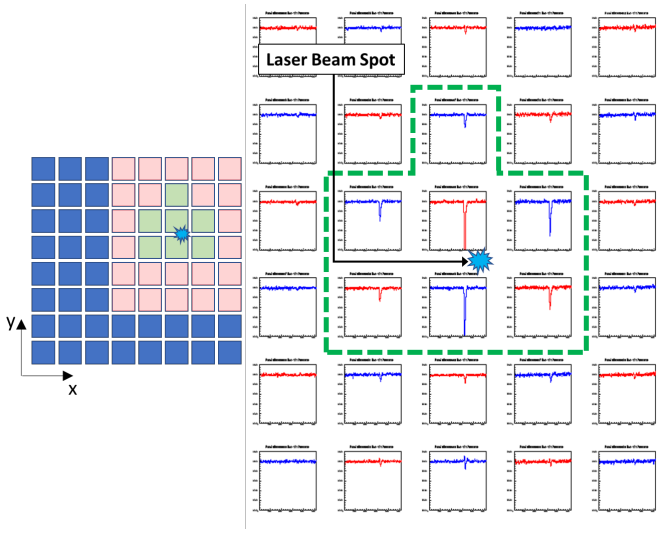

Figure 3 The array of digitized waveforms (50 ns full scale) on the right corresponds to the subset of pink 6 mm × 6 mm pixels on the left. Signal generated by the laser beam spot on the green pixels survived the amplitude threshold cut and define a charge cluster.

Figure 4 shows a different representation, for 3 mm square pixels. In both cases one can see good charge sharing, which – as will be shown later – is sufficient for measuring the position with accuracy much better than a pitch / √12 estimate.

B. Crosstalk

Crosstalk measurements were also performed in the lab to gauge the importance of this effect, which may be potentially harmful in the case of interleaved strips due to increased strip-to-strip capacitance. To help alleviate this effect, signal traces in

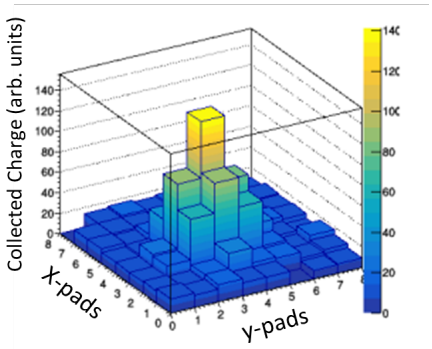

Figure 4: The 2D charge distribution resulting from the detection of a single photon on a 8 × 8 3mm square pixel array. The RMS width is ~3.5 mm in both projections.

the readout PCB stack are designed in a 50 Ohm coplanar waveguide configuration, in order to preserve induced pulse integrity and suppress a crosstalk. The traces from neighboring pixels are spatially staggered and separated by ground planes in the PCB stack-up. As shown in Figure 5, signals induced in neighboring pads are relatively small in amplitude and account for only a few % of the main signal, in the worst-case scenario. A similar response was also observed for the interleaved anode pixels described below. Ultimately, crosstalk was found to have a minimal effect on all of results reported here.

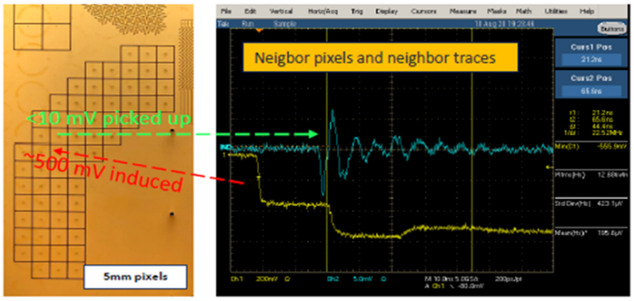

Figure 5: Charge from a 500mV amplitude square pulse (i.e., the yellow oscilloscope trace) is injected directly onto a single readout pad of the shown pixel array. The resulting pickup from a closest neighbor pad corresponds to a small <10mV signal (i.e., the blue oscilloscope trace).

C. Linearity of Response and Position Resolution

The centroid suffers a very small systematic offset from the actual beam spot position as the beam is scanned diagonally across the readout, as shown in Figure 6. The resulting position resolution, taken as the width of the residual distribution is typically below 500 μm, as shown in Figure 7. Though the linearity of response across the readout is quite good, due to the relatively small signal amplitudes, the noise to signal ratio is a main limiting factor for the position resolution.

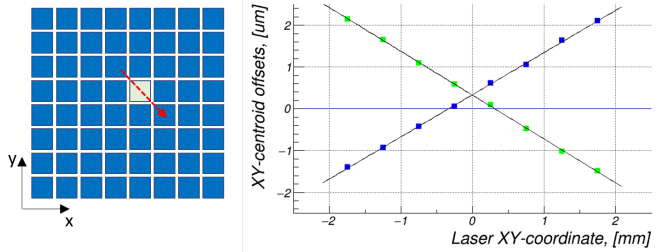

Figure 6: The centroid offset determination (right) from a laser scan along the diagonal of a 4 mm x 4 mm area (centered on the green pad) of a pixelated anode pattern consisting of 3 mm × 3 mm square pads (left). The blue and green points correspond to x-and y-coordinate measurements, respectively.

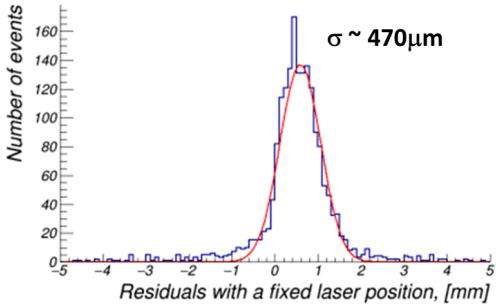

Figure 7: The residual distribution produced from the 3mm pixelated anode pattern.

D. Interleaved Anodes

In an effort to maintain a similar level of performance with a substantial reduction in channel count, 2D interleaved anode patterns, as shown in Figure 8 were also employed for the readout. In place of square pads, these "interleaved pixels" were initially used to evaluate the basic performance of this anode concept. The blue interleaved pixel is efficient at sampling the charge cloud along the vertical (y) direction and the red pixel is better at sampling charge along the horizontal (x) direction. Due to the interleaving nature of these anodes, multiple red-like and blue-like interleaved pixels are thus able to effectively sample the same charge cloud to provide a 2D coordinate measurement of the photon impact point.

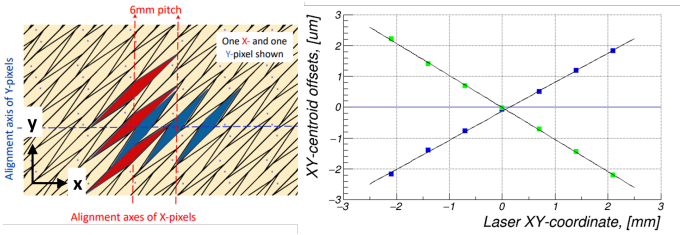

Figure 8: The group of three red diamond-shaped anode elements on the left panel are electrically connected in the inner PCB layers and effectively form a single pixel that covers a 6 mm × 6 mm area. The blue anode elements similarly make up a similar interleaved pixel, but oriented horizontally. The plot on the right shows the centroid offset determination from a diagonal laser scan across the interleaved pixel anode pattern.

A similar diagonal scan with the laser beam was performed for this anode pattern and also shows a highly linear response. However, the residual distribution reveals a position resolution of about 700 μm as seen in Figure 9.

The significantly larger pitch of the interleaved pixels compared to the square ones is a main contributing factor for the

difference in the observed resolution in Figures 7 and 9. However, another important contributing factor is the fact that effectively only half of the charge is used to make a centroid determination along each projection. If the charge from neighboring interleaved pixels was combined to calculate the resolution along a single projection at a time, as in the case of the square pixels, the resolution then approached 500μm.

The rationale behind splitting charge between X- and Y-projections is the following. *If occupancy limits allow, sets of interleaved pixels may be horizontally and vertically chained to form interleaved anode strips to provide 2D information with the same resolution performance and linearity of response, but with far fewer channels.* Thus, instead of pad arrays, two sets of 1D strip segments may be organized on a single readout plane to simultaneously measure two orthogonal coordinates with a spatial resolution below 1 mm. It is worth mentioning that (contrary to square pads of the same footprint) the induced signal is split very evenly (to within a few %) between x and y projections in the case of the interleaved pixels. Given the fact that LAPPD single photon amplitudes have a substantial spread, this circumstance must also be helpful in resolving ambiguities in a high occupancy environment.

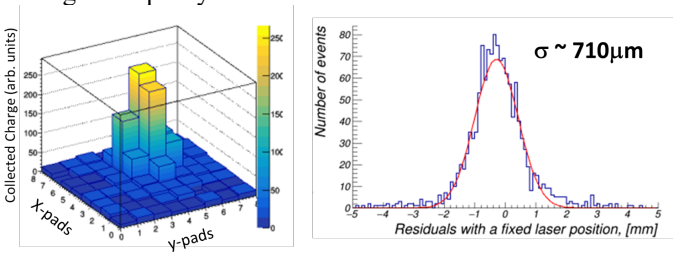

Figure 9: 2D charge distribution response of a 2D interleaved anode pattern with 6 mm pitch due to a single photon (left) and the resulting residual distribution (right).

IV. Beam Test Results

The equipment was later brought to the Fermilab Test Beam Facility (FTBF) [6] to study the performance of the same LAPPD setup with 120 GeV protons. In this case, a thick 20 mm focal length aspheric fused silica lens was used as a radiator to generate Cherenkov photons that impinge the LAPPD photocathode.

A. Setup at Beam Test

A photo and schematic of the beamline setup is shown in Figure 10, which consists of a pair of scintialltion counters and the same LAPPD lab stand and enclosure. A two-way coincidence trigger was organized using the two scintillation counters to provide a global timing trigger for the DAQ. Additionally, the same voltage configuration and DAQ that was used in the lab was employed during the beam test. Figure 10 shows the position of the aspheric lens in relation to the particle beam, the LAPPD, and the emerging Cherenkov photons. The particle beam first passes through the LAPPD and the acrylic filter, then enters the lens radiator where Cherenkov photons are generated. The photons reflect off the rear flat surface of the lens due to the total internal reflection, undergo a refraction into air on the concave lens surface and a sequence of further refractions on the optical boundaries between air, acrylic filter and LAPPD fused silica window. Simualtions show that in this configuration, due to the fact that the effective imaginary Cherenkov photon source is located far enough from the central part of the concave lens surface (behind the flat side), most part of the photons contribute to the ring image rather than become a stray background after several unwanted reflections inside the lens. An acrylic filter is installed as a safety measure to provide a cutoff at small wavelengths where the refractive index of fused silica exhibits a substantial variation as a function of wavelength.

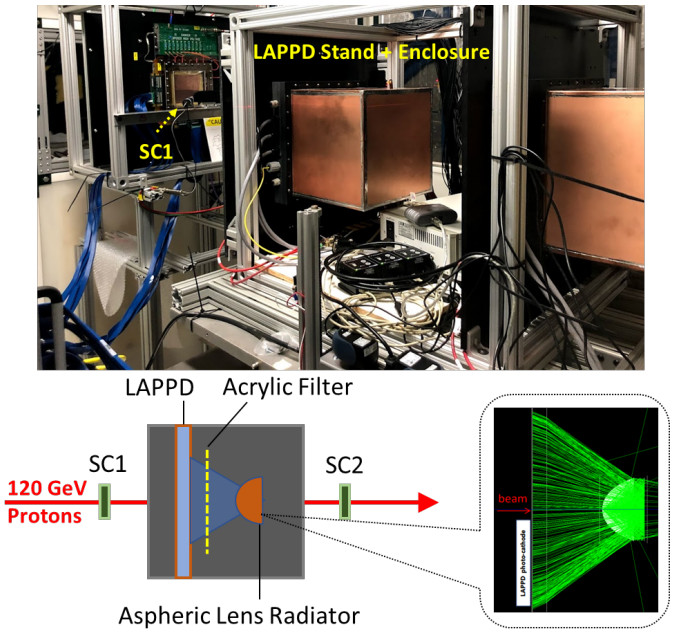

Figure 10: Photo of the beamline setup for the LAPPD measurements using an aspheric lens radiator (top). A schematic of the beam line elements is shown at the bottom, where "SC1" and "SC2" designates the two scintillation counters used in the setup.

The particle beam profile is roughly 1 cm × 1 cm with a divergence of a few hundred microradians. Due to the focussing nature of the aspheric lens, Cherenkov photons, for the primary 120 GeV proton beam all emitted at a saturation angle of ~47^0 to the primary particle direction, end up at the same radial position on the focal plane with respect to the lens axis, regardless of their emission point in the lens fused silica material. Therefore, there is no need for a primary proton tracking system. Rather, the relevant direct measure of the position resolution in this case is the uncertainty in the radius of the reconstructed Cherenkov ring itself on a photon-by-photon basis, with respect to the lens optical axis. The paramaters of the latter can be established experimentally with a high accuracy from the same data set.

B. Results

A single event display showing the charge generated in the LAPPD by Cherenkov photons produced by a passage of a single proton through the aspheric fused silica lens is shown in Figure 11.

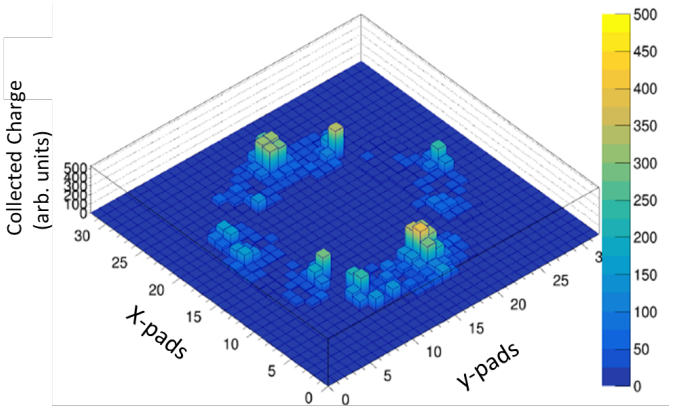

Figure 11: Single event Cherenkov ring of a ~76 mm diameter with multiple photon clusters measured with the LAPPD detector coupled to an aspheric lens radiator.

The crispness of the reconstructed ring, consisting of multiple photon clusters, indicates the position resolution with which this device can image single photons, a crtitical perfromance factor for most RICH applications. Unlike the laser tests in the lab which dealt with one photon per event, mulitple clusters appear on the readout at once due to the generation of multiple Cherenkov photons. As a result, a more sophisticated recursive clustering algorithm is employed here based on a topologic search method, which allows to disentangle continuous charge distribution into individual clusters corresponding to single photons. The weighted mean centroid calculation for every individual cluster is the same as with the laser setup. Figure 12 shows the resulting scatter of each reconstructed photon position on the reference plane, integrated over many events, and reveals a very narrow effective ring width.

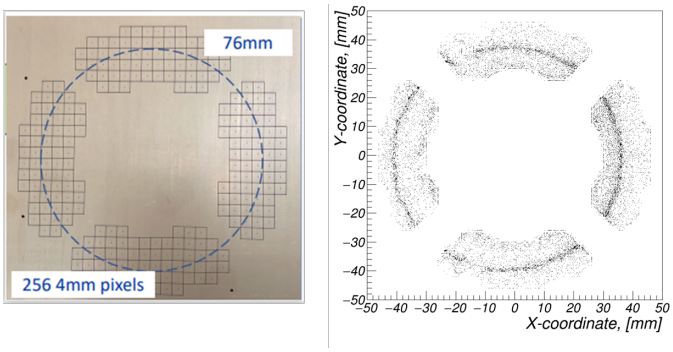

Figure 12: The centroid XY-distribution derived from single photon clusters integrated over many events (right) using a 4 mm × 4 mm pixelated square pad readout (left). The readout board in this case was designed such to strategically place 256 available DRS4 channels along the expected Cherenkov ring circumference matching the aspheric lens optics. Apparent ring image center corresponds to the location of the lens, which was accidentally displaced in the experiment with respect to the pad pattern by ~2.5 mm horizontally and ~1.0 mm vertically.

The 1D distributon of the measured ring radii is plotted in Figure 13 (left) and shows a ring width substantially less than 1 mm, consistent with the spatial resolutions measured in the lab. As a proof of principle measurement, the aspheric lens was placed in and out of the beam to explicitly demonstrate the sensitivity to Cherenkov light. With the lens out of the beam, the residual distribution is flat, equal to the baseline in the left plot for the same number of triggers, and likely originates from stray and background photons.

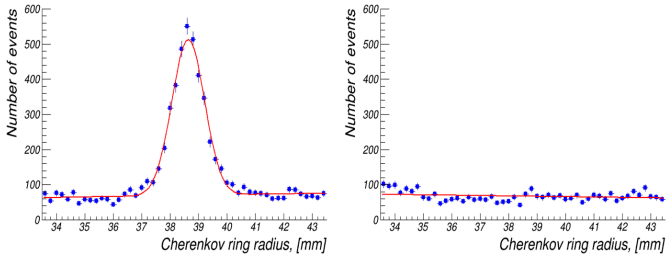

Figure 13: The distribution of single photon Cherenkov ring radii, measured over many events with the aspheric lens in place (left) and moved out of the beam (right). The sigma width of the radii distribution is ~580 μm. This number represents an upper limit on the intrinsic pixelated LAPPD spatial resolution in this setup, since no attempt was made to unfold contributions of the lens fused silica refractive index variation over LAPPD photon detection efficiency wavelength spectrum, beam angular divergence, lens geometry imperfections and other instrumental effects.

V. Summary

We have investigated the spatial resolution of a Gen II LAPPD detector coupled to an external capacitively coupled readout plane. Measurements were carried out both in the lab environment using a focused picosecond laser beam and at a beam test facility with a fused silica radiator exposed to a high energy particle beam. A sub-mm spatial resolution was achieved in the lab with a very high degree of linear response for single photons using a traditional 3 mm square pixelated readout. A similar result was also achieved in the lab using 6 mm 2D interleaved pixel anodes that have the potential for being formed into strips that deliver the same performance, but with far fewer readout channels. Our experience with the interleaved anodes for gaseous detectors [7,8,9] indicates that (given the induced LAPPD signal spread) the pitch of the interleaved anode strips may also be substantially increased to reduce the channel count while maintaining the resolution performance. Finally, once coupled to an aspheric lens radiator, Cherenkov rings measured during a beam test were reconstructed with a single photon resolution equal to ~600 μm. The timing characteristics of the LAPPD detector for ToF applications will be reported on in a future publication.

VI. Acknowledgements

We would like to thank the staff at the FTBF, including Mandy Rominsky, Evan Niner, Eugene Schmidt, and Todd Nebel for their support and expertise during the beam test campaign.

VII. References

[1] B. Adams et al., “A Brief Technical History of the Large-Area Picosecond Photodetector (LAPPD) Collaboration”, arXiv:1603.01843 (2016)

[2] https://incomusa.com/lappd

[3] B. Adams et al., “Timing characteristics of Large Area Picosecond Photodetectors”, Nucl. Instrum. Meth. A795 (2015) 1

[4] A. Lyashenko et al., “Performance of Large Area Picosecond Photo-Detectors”, Nucl. Instrum. Meth. A958 (2020) 162834

[5] E. Angelico et al., “Capacitively coupled pickup in MCP-based photodetectors using a conductive metallic anode”, Nucl. Instrum. Meth. A846 (2017) 75

[6] C. Wong et al., “Modular focusing ring imaging Cherenkov detector for electron-ion collider experiments”, Nucl. Instrum. Meth. A871 (2017) 13

[7] B. Azmoun et al., “Design Studies of High-Resolution Readout Planes using Zigzags with GEM Detectors”, IEEE Trans.Nucl.Sci. 67 (2020) 8, 1869.

[8] A. Kiselev, “2D charge sharing readout planes for GEM, μRWELL and other detector applications”, TIPP 2021 virtual conference.

[9] M. Revolle et al., “Performance of the μMegas and μRWELL detector prototypes equipped with the modern laser etched readout planes with improved charge sharing properties”, MPGD 2019 conference (La Rochelle, France).